Research Article Vol. 2, No. 9 / 15 Sep 2023 / Optics Continuum 1901
OPTICS CONTINUUM

Towards fiber-coupled plasmonic perfect absorber superconducting nanowire photodetectors for the near- and mid-infrared

SANDRA MENNLE,* PHILIPP KARL, MONIKA UBL, PAVEL RUCHKA, KSENIA WEBER, MARIO HENTSCHEL, PHILIPP FLAD, AND HARALD GIESSEN

4th Physics Institute and Research Center SCoPE and IQST, University of Stuttgart, Pfaffenwaldring 57, 70569 Stuttgart, Germany
*Sandra.mennle@pi4.uni-stuttgart.de

Abstract: Modern photon-based technologies are in need for fast detectors with the ability to detect photons in the near- and mid-IR efficiently. Superconducting nanowire photon detectors, which use the resistivity change upon photon incidence caused by a state transition from their superconducting to normal conducting phase, are state-of-the-art detectors. However, detectors usually suffer from low efficiency in the IR, due to their low intrinsic absorption in this spectral range. To enhance the detection efficiency, we use a plasmonic perfect absorber geometry, which utilizes a localized surface plasmon resonance and a spacer/mirror combination. We present superconducting niobium plasmonic perfect absorber nanostructures, featuring near-unity absorption, tailorable up to wavelengths of 4 μm. Further, we confirm the working principle of the plasmonic perfect absorber for wavelengths in the near-IR, which manifests itself as a polarization-dependent detector response. Finally, we demonstrate an approach of coupling the detector directly to a fiber. This might also enable ultrasensitive sensing application in the near- and mid-IR in the future.

1. Introduction

Photon-based quantum technologies, such as quantum computing [1], quantum sensing [2], and quantum cryptography [3] are a growing field of research, which requires fast, efficient and reliable photon detection. Moreover, there are many applications for small and highly sensitive IR photodetectors, e.g., for spectroscopy [4], data transmission in the telecom band [5], and IR space telescopes [6]. Promising candidates that fulfil these requirements are superconducting photon detectors e.g. superconducting nanowire single photon detectors [7,8] or superconducting transition edge detectors [9], which change their resistivity under light incidence, due to a phase transition from the superconducting to the normal conducting state. Depending on the area of application, commonly used superconducting materials are niobium titanium nitride [10,11,12], tungsten silicide [13], and niobium nitride (NbN) [14,15].

However, the intrinsic absorption of commonly used superconducting metals, e.g. niobium (Nb) and NbN is low, especially for wavelengths in the mid-infrared (MIR) spectral range. One way to enhance the absorption is to aim for a larger active area. However, such a detector has bigger kinetic inductance and thus, a longer recovery time [14]. Therefore, various other approaches, such as waveguides [16] and cavities [17] have been developed to enhance this absorption. Another concept is utilizing plasmonic resonances, which can be found in various applications [18,19,20]. These resonances feature a high resonant absorption cross-section, which allows for small active areas with high absorption nonetheless. In contrast to cavities,

#496334 https://doi.org/10.1364/OPTCON.496334
Journal © 2023 Received 24 May 2023; revised 7 Aug 2023; accepted 10 Aug 2023; published 23 Aug 2023

OPTICS CONTINUUM

they show an angle of incidence insensitivity [21,22], which opens the possibility for using high NA focusing optics to reduce the light spot size and therefore make even smaller detector areas possible.

To enhance the absorption even further, a plasmonic perfect absorber geometry [23,24,25] can be used. By confining the incident light in the active material, near-unity absorption can be reached, which has already been demonstrated for various applications, e.g., photodetection [26,27] or sensing [21,28].

In this work a superconducting nanowire photodetector with a plasmonic perfect absorber geometry is presented, utilizing Nb as active material, which exhibits a near-unity absorption in the IR spectral range. The plasmonic enhancement of the detector response to light incidence is demonstrated by polarization sensitive measurements. Finally, we present an approach to couple the incident photons more efficiently to the detector, by using 3D-printed microstructures.

2. Design and simulations

Plasmonic perfect absorbers are a special kind of structures, which utilize a localized surface plasmon resonance to confine incident light and therefore lead to unity absorption. In Fig. 1(a) a schematic sketch of a perfect absorber geometry is depicted: On top of the substrate a 120 nm thick gold mirror is placed, followed by a dielectric spacer layer, which is aluminum oxide (Al_2O_3) for our samples. The topmost layer consists of a 50 nm thick Nb film, which is nanofabricated into a nanowire array. The Nb film is hereby sputter-deposited at ambient temperature in a Pfeiffer 570 at 5×10^{-8} mbar and at 25 sccm argon gas. If now photons are incident, their electric field excites an oscillation of the charge carriers in the Nb nanowires, forming a so-called localized surface plasmon. Due to Coulomb forces an antisymmetric oscillating mirror plasmon is evolving in the gold layer. We can understand these moving charges as a ring current, which generates a magnetic mode. This magnetic mode than can interact with the magnetic field of the incident light. If the geometry is tuned right, i.e., the effective surface impedance $Z_s = (\mu/\varepsilon)^{1/2}$ of the structure equals the vacuum impedance of $Z_v = 1$, it will result in a reflection of 0, due to $R = |(Z_v - Z_s)/(Z_v + Z_s)|^2$. In addition, the thick gold layer suppresses any transmission T in the IR spectral range. Thus, one ends up with unity absorption A = 1 - R - T = 1 [28]. To obtain this perfect absorption, the geometry of the perfect absorber can be optimized by adjusting the wire width, the period, and the thickness of the Al_2O_3 layer.

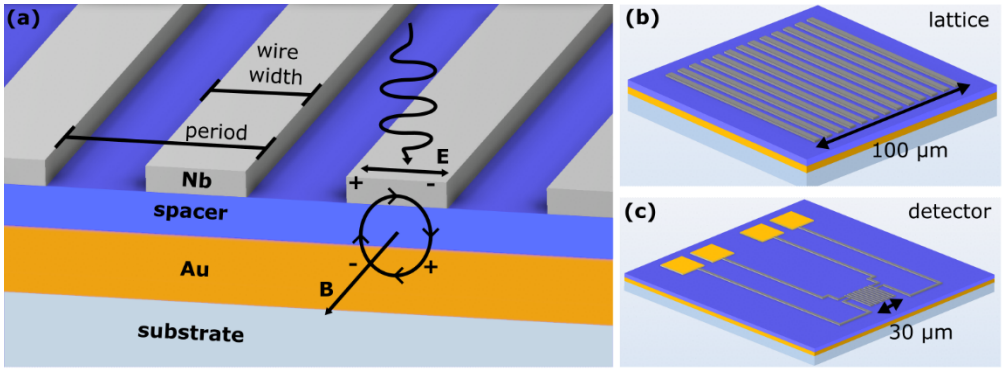

Fig. 1. Working principle of the plasmonic perfect absorber and design. (a) Sketch of a plasmonic perfect absorber structure with Nb as active material. Incident light excites a plasmon oscillation in the nanowire, which leads to an antisymmetric oscillating mirror plasmon in the gold layer. The moving charges generate a ring current and induce a magnetic mode, which interacts with the magnetic field of the incident light. (b,c) Designs of test-lattice and the final detector.

OPTICS CONTINUUM

However, the perfect absorption only works if the incident light is polarized perpendicular to the wires (TM polarization). The absorption of the nanowire in TE polarization along the wires is caused mostly by the intrinsic absorption of the metal.

In Fig. 1(b) and (c) the design of our perfect absorber nanostructures is shown. The design in (b) will be called a 'lattice' in the following and consists of parallel nanowires, forming a square with an area of $(100 \times 100)\ \mu m^2$. Due to its large size and simplicity, it is used to perform a large number of absorption measurements, while changing the geometry. In Fig. 1(c) the design of the actual detector is shown: To form a single, continuous wire, the nanowires are connected at alternating ends. Moreover, the $(30 \times 30)\ \mu m^2$ active area is connected to gold contact pads with a side length of 250 µm, to which the detector is bonded with gold wires to a standard chip carrier.

Before the actual fabrication of the lattices, simulations are carried out to find the optimal parameters. To do so, an in-house implementation utilizing the Fourier modal method with a scattering matrix approach and 225 plane waves is used [29,30]. To make the simulations as accurate as possible, the refractive index of a 50 nm Nb film is measured with ellipsometry and extrapolated to higher wavelengths according to the Drude model (see Fig. 6 in Appendix). In Fig. 2 the resulting simulated absorption spectra are shown for a varying wire width between 500 nm and 1750nm for two different periods (1500 nm (Fig. 2(a)) and 2500 nm (Fig. 2(b)). The spacer layer consists of 100 nm Al_2O_3 and the thickness of the Nb film is 50 nm. The simulations are performed for TM polarization, which is perpendicular to the wires, as depicted in Fig. 2(c). In the simulated spectra a typical plasmonic resonance with near-unity absorption absorption in the Nb-wire (proven by the field distribution in Fig. 7 in the Appendix) can be observed. The resonance is broadband and its spectral position can be shifted over a wide spectral range by changing the wire width. We can understand this behavior by imagining the nanowire as a dipole antenna: To be resonant to a certain wavelength, the wave must spatially fit into the nanowire. However, to sustain the high absorption over the whole range the period needs to be optimized, too. These results prove that with the concept of the plasmonic perfect absorber one is able to reach an absorption of almost 100% for wavelengths far into the MIR. For wavelengths beyond 8000 nm the used spacer becomes absorbing due to a phonon resonance, so one needs to replace the spacer material, for example with germanium, to extend the perfect absorber even further.

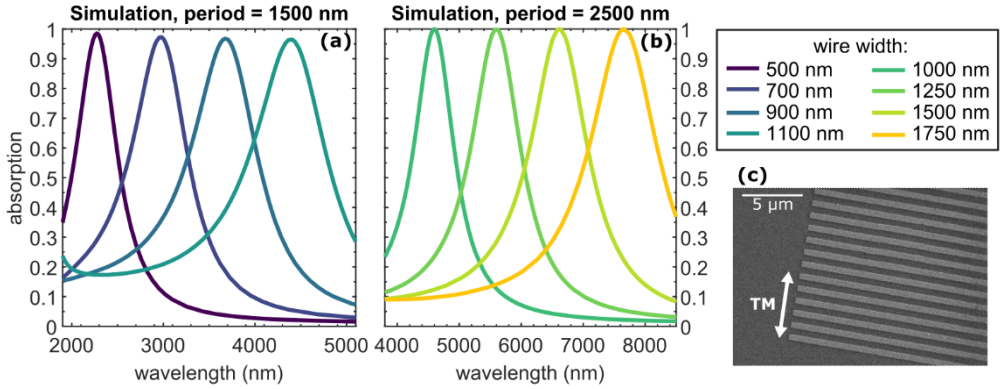

Fig. 2. Simulated absorption of perfect absorber lattices for varying wire widths and periods of (a) 1500 nm and (b) 2500 nm. The simulation shows near unity absorption, which can be shifted over a wide spectral range up to wavelengths of 7500 nm with changing the wire width and adjusting the period. Please note that the period is deep subwavelength, so no grating effects or Rayleigh-Wood anomalies occur. (c) SEM image of a plasmonic lattice to depict the used polarization.

OPTICS CONTINUUM

3. Absorption and electric response measurements

In Fig. 3 measurement results of fabricated perfect absorber lattices with varying period, wire width, and spacer thickness are displayed. The spectra are obtained with a Fourier-transform infrared spectrometer (FTIR) measurement (Bruker Vertex 80 microscope Hyperion 3000) under normal incidence. As a reference, the gold mirror with the Al_2O_3 layer next to the lattice structure is used. In Fig. 3(a) we plot the absorption in dependence of the wavelength for different wire widths between 350 and 1000 nm in TM polarization. For the three smaller widths the period of the lattice is 1000 nm and the spacer thickness is 100 nm; for the largest wire width we use a period of 1600 nm and a spacer thickness of 140 nm. The data depict a plasmonic resonance with an absorption of 97%, whose center wavelength is tunable over a wide spectral range from 2000 to 4000 nm by adjusting the width of the nanowires. In the figure, we also illustrate the measured absorption in TE polarization along the wires for the lattice with 1000 nm wire width. In this polarization the IR light cannot excite any plasmons, thus, only the intrinsic absorption of the Nb layer remains and contributes to the low absorption of 15% at 4000 nm wavelength. Compared to the absorption in TM polarization we therefore reach a plasmonic enhancement factor of over six.

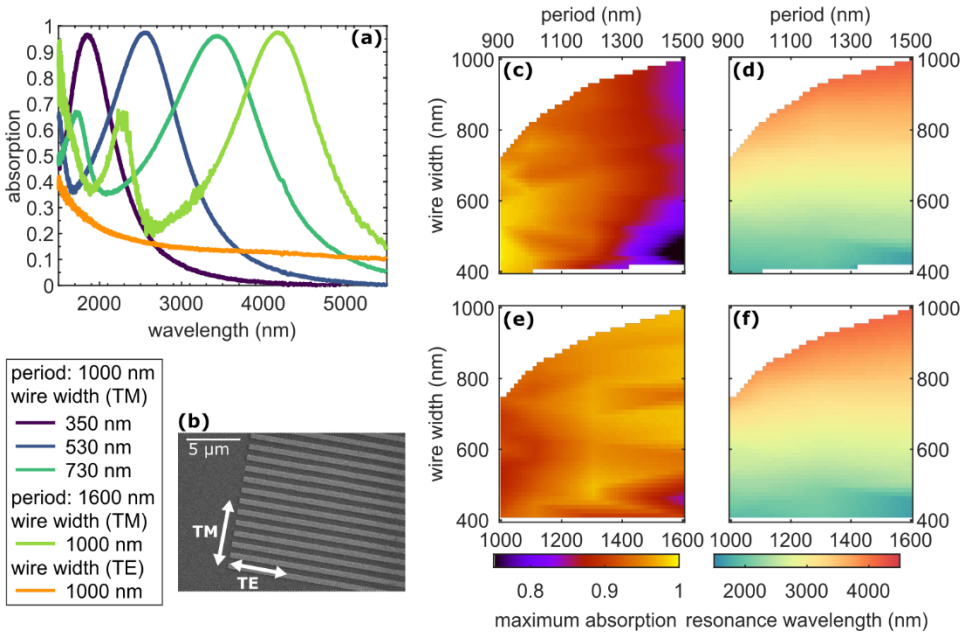

Fig. 3. Measured absorption of perfect absorber lattices. (a) The spectra show broadband, near-unity absorption, which can be tuned over a wide spectral range far into the mid-IR. Moreover, the absorption in TE polarization is shown. Due to the lack of plasmon excitations, the absorption is smaller. (b) SEM image of one of the used lattices with polarization definitions. (c-f) Heatmaps of the maximally achieved absorption (c,e) as well as the resonance wavelength (d,f) in dependence of the wire width and the period of the lattice. For (c) and (d) the spacer thickness is 100 nm and for (e) and (f) it is 140 nm. The pictures demonstrate that the resonance wavelength is only dependent on the wire width, while for near unity absorption the period and spacer thickness need to be optimized.

For the data displayed in Fig. 3(c)-(f) we extracted the maximal obtained absorption (c,e) as well as the resonance wavelength (d,f) from measured spectra for various wire widths and periods and plot them as interpolated heatmaps. For Fig. 3(c) and (d) we use a spacer thickness of 100 nm and for Fig. 3(e) and (f) a thickness of 140 nm. Figure 3(d) and (f) illustrate the same

OPTICS CONTINUUM

behavior as in (a), namely a widely spectrally tunable resonance. Increasing the wire width will hereby also increase the resonance wavelength of the plasmonic perfect absorber. The plot also proves that the influence of changing the period or the spacer layer thickness on the spectral position of the resonance is negligible. However, they do have an influence on the strength of the resonance, i.e., the maximum absorption, which is demonstrated in Fig. 3(c) and (e): Resonances at lower wavelengths (e.g., 2500 nm) require a smaller period and a thinner spacer layer to exhibit high absorption. For higher wavelengths the perfect absorber geometry needs to be scaled up.

To test the benefits of the plasmonic perfect absorber for photon detection, we fabricate a detector and test its response to photon incidence under cryogenic conditions. Following the results in Fig. 3 we manufacture the detector with a period of 900 nm and a wire width of 410 nm, which results in a resonance with 90% absorption at our target wavelength of around 2000nm in TM polarization, as depicted in Fig. 4(a). Moreover, we benefit from a second resonance at a wavelength of around 1200 nm, which lets us test the plasmonic behavior at a smaller wavelength first, before measuring at our target wavelength. In the plot, we also show the absorption in TE, which represents the intrinsic absorption of the Nb wires. Compared to the absorption spectra of the lattices, the TM as well as the TE absorption curve show a good match. In Fig. 4(b,c) the response of the detector to light incidence is shown. In the experiment the detector was cooled down in a cryostat to around 2 K, a bias current was applied with a Keithley 2611B current source and the change of the voltage drop under light incidence was measured. This response can be understood as follows: If incident photons are absorbed by the Nb nanowire, their energy causes a breaking of the Cooper-pairs in a small hot-spot region, which becomes normal conducting. Due to its higher resistivity, the bias current is forced to flow around that hot-spot. This exceeds the critical current density in the area surrounding the hot-spot and leads to breaking of the Cooper-pairs there as well. This avalanche-like effect then continues and one can measure a non-vanishing resistivity.

For the measurements in Fig. 4(b) and (c) the sample is illuminated in a free-space setup through a cryostat window. The alignment and focusing of the laser spot onto the detector is carried out with the help of a CCD camera. In Fig. 4(b) we use a cw-laser with a wavelength of 1140 nm, apply a bias current of 700 µA and plot the signal over the power of the attenuated laser. The data exhibit a bigger signal in TM polarization than in TE polarization, due to a higher absorption. This is especially true for low laser powers below 5 µW, as depicted in the inset. In this power range, the detector response was almost doubled in TM polarization, because the plasmonically enhanced absorption increases the detection efficiency. One should also notice that in TM polarization a laser power as small as 1 µW could be detected, which was not possible in TE polarization. Currently, detector responses below approx. 0.01 µV are not detectible with the used setup, due to electric noise, e.g., external noise from unshielded cables and noise from the electric devices. We are working on improving the setup, so in the future smaller signals could be detected. For high laser powers above 75 µW the response becomes polarization-independent, since the power is so large that we are heating the detector above the critical temperature and therefore do not benefit from the plasmonically enhanced absorption anymore. Moreover, at these high powers, the measured response curve saturated, because the detector is now mostly normal conducting and the probability that all photons are absorbed in a superconducting area is reduced. In Fig. 4(c) the light source is switched to a pulsed laser (Stuttgart Instruments Alpha HP) with 2000nm wavelength, a repetition rate of 20 MHz, and 200 µW average power. We plot the signal in dependence of the applied bias current. Due to the long wavelength, alignment with the CCD-camera is not possible and therefore the correct position and focus cannot be confirmed easily. The measured signal exhibits a maximum at a bias current of 800 µA. If the bias current is lower, the energy of the incident photon is not big enough to trigger the state transition over the entire wire width, due to the lack of the avalanche-like effect. If it is too high, part of the detector is already normal conducting even without photon incidence, due to defects in the nanowires.

OPTICS CONTINUUM

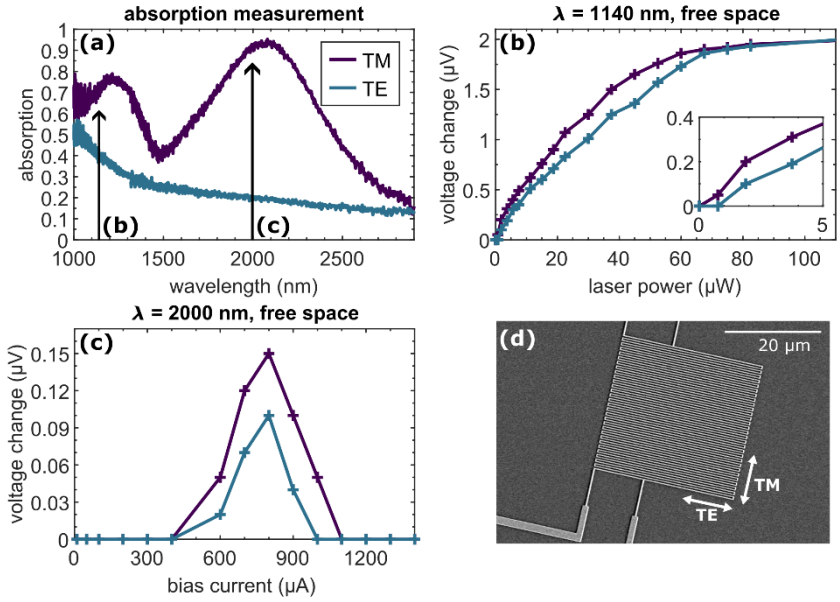

Fig. 4. Absorption and electric response of a (30×30) μm^2 detector with a period of 900 nm and a wire width of 410 nm, illuminated via free-space. (a) Polarization-dependent absorption spectra of the detector. In TM polarization the data indicate a resonance with 95% absorption at 2000nm as well as a second smaller resonance at 1200 nm. (b) Measured signal, manifested as a voltage change uppon light incidence, in dependence of the laser power and polarization at a wavelength of 1140 nm. The bias current was 700 μA. The detector exhibits a larger response in TM polarization caused by the plasmonically enhanced absorption. (c) Voltage change in dependence of the applied bias current for TM and TE polarization at 2000nm wavelength. In this measurement the laser power is set to 200 μW. The maximum detector response arises at 800 μA. At lower currents the state transition of the detector is not triggered, and at larger currents some parts are already normal conducting without photon incidence. The picture confirms a polarization dependent detector response which proves the plasmonic enhancement in MIR. (d) SEM image of a detector with marked polarizations.

Both will lead to a decreased detector response. The data display a bigger response in TM polarization while the identical laser power was applied, resulting in an excitation ratio of 1. This proves that the concept of the plasmonic perfect absorber works fine at higher wavelengths.

4. Fiber-coupled detectors

Precise free-space alignment between laser spot and detector is challenging for larger IR wavelengths, since one has to use thermal imaging devices. To enhance the coupling efficiency by improving this alignment, we couple the detector directly to a single-mode fiber. Figure 5(a) shows a schematic sketch of how this is achieved: On top of the finished detector, we 3D-printed (Nanoscribe Professional GT 3D printer) a fiber chuck [31]. Figure 5(b) depicts a microscope image of the chuck. In the image the detector and the connections to the contact pads are also visible. Afterwards, a fiber is cleaved and inserted into the central hole of the fiber chuck. Finally, fiber and chuck are glued together with UV glue (Norland optical adhesive 63). An image of the finished sample with an attached fiber is depicted in Fig. 5(c).

In Fig. 5(d) we plot the measured response over the average laser power at a wavelength of 2000nm with the fiber-coupled detector. The inset shows the response in dependence of the

OPTICS CONTINUUM

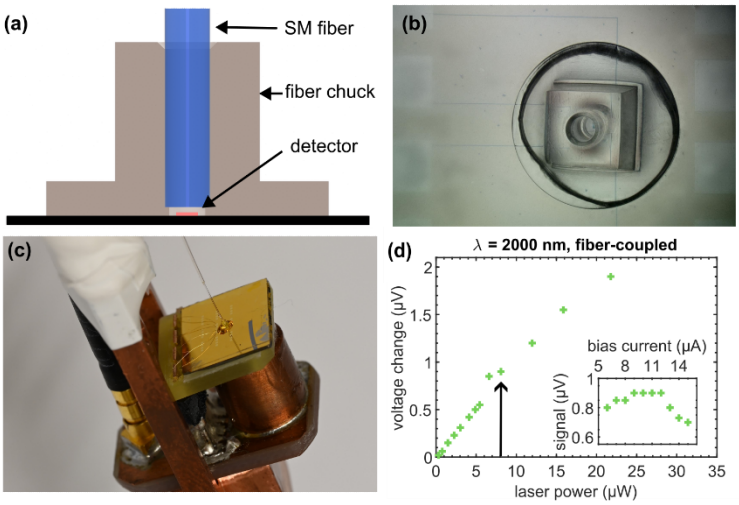

Fig. 5. Fiber-coupled detector. (a) Drawing of the hollow fiber chuck with the fiber inserted. After aligning, the fiber is glued with UV-glue. (b) Microscope image of the fiber chuck. (c) Image of a finished fiber-coupled detector device on the sample holder. In the figure, the fiber chuck with the attached fiber is shown. Moreover, the bonding wires and the bonding pads are visible. (d) Measured voltage change in dependence of applied laser power at a wavelength of 2000nm and a bias current of 11 mA. Due to better focusing and aligning, a substantial signal increase was achieved when compared to the free-space-setup. (inset) For obtaining the optimal bias current, we plot the voltage change over the bias current while using a laser power of 8 μW.

applied bias current for a laser power of 8 μW. For this measurement, a bias current of 11 mA results in the largest signal. This increase, compared to the free-space measurement in Fig. 4(c), is caused by changing the setup and using a different sample (but with the same fabrication parameters). Since we used a non-polarization-maintaining fiber, we cannot perform polarization-dependent measurements with this setup. In the future, one could use a polarization-maintaining fiber to solve this issue. The data confirm that with fiber-coupling we were able to detect laser powers below 1 μW, which was not possible before. Moreover, compared to the free-space setup, we gain a huge overall signal increase, which is caused by the better alignment and better focusing by utilizing the fiber.

5. Conclusion and outlook

In this work we presented superconducting photodetector for the infrared spectral range, which use niobium as active material. Utilizing a plasmonic perfect absorber geometry we demonstrated near-unity absorption, which is tailorable over a wide spectral range far into the mid-IR. Moreover, we demonstrated a polarization-dependent detector response upon light incidence, which indicated that our plasmonic perfect absorber geometry indeed leads to signal enhancement and hence to a higher detection efficiency, which opens the way towards highly sensitive photodetection down to the single photon regime. In addition, we demonstrated a concept for improving the alignment between detector and incoming light by coupling the detector directly to an optical fiber, which resulted in a large signal increase. Since detectors with a perfect absorber geometry also work well for large angle of incidences and due to the high precision of 3D-printing [32], this can be used in the future to fabricate smaller, and therefore faster detectors by utilizing fibers with high-NA optics.

OPTICS CONTINUUM

6. Appendix

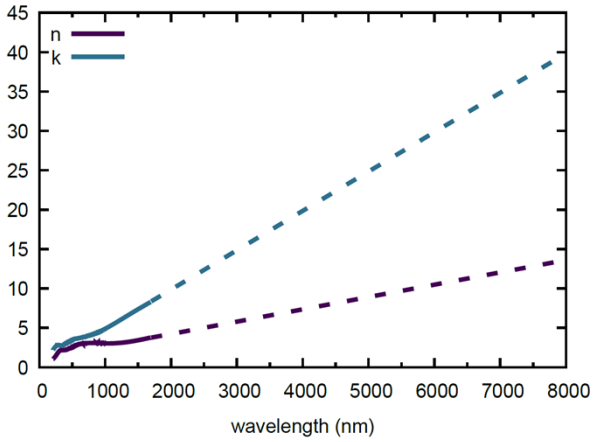

Fig. 6. Refractive index of our 50 nm thick Nb film on a perfect absorber substrate. The solid lines depict measured data, the dashed data are extrapolated linearly according to the Drude model.

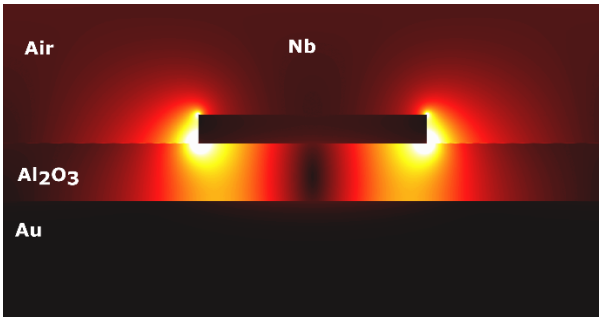

Fig. 7. Simulated electric field distribution of a Nb nanowire on top of a perfect absorber substrate upon incidence of resonant light with a wavelength of 2000nm. Since there is only a vanishing field inside the gold layer, most of the incident energy is absorbed inside the Nb nanowire.

Funding. Open Access Fund University of Stuttgart; Center for Integrated Quantum Science and Technology (IQST); Ministerium für Wissenschaft, Forschung und Kunst Baden-Württemberg; Baden-Württemberg Stiftung; Carl-Zeiss-Stiftung; Deutsche Forschungsgemeinschaft; European Research Council.

Acknowledgments. We thank T. Weiss from the Institute of Physics (University of Graz) for help with the S-Matrix simulations and M. Floess (University of Stuttgart), T. Steinle (University of Stuttgart) and his colleges from Stuttgart Instruments for help with the laser systems.

Disclosures. The authors declare no conflicts of interest.

Data availability. Data underlying the results presented in this paper are not publicly available at this time but may be obtained from the authors upon reasonable request.

References

1. J. L. O'Brien, "Optical Quantum Computing," Science **318**(5856), 1567–1570 (2007).
2. C. L. Degen, F. Reinhard, and P. Cappellaro, "Quantum sensing," Rev. Mod. Phys. **89**(3), 035002 (2017).
3. R. J. Hughes, D. M. Alde, P. Dyer, G. G. Luther, G. L. Morgan, and M. Schauer, "Quantum cryptography," Contemp. Phys. **36**(3), 149–163 (1995).

OPTICS CONTINUUM

4. J. Haas and B. Mizaikoff, "Advances in Mid-Infrared Spectroscopy for Chemical Analysis," Annu. Rev. Anal. Chem. **9**(1), 45–68 (2016).
5. B. Corcoran, M. Tan, X. Xu, A. Boes, J. Wu, T. G. Nguyen, S. T. Chu, B. E. Little, R. Morandotti, A. Mitchell, and D. J. Moss, "Ultra-dense optical data transmission over standard fibre with a single chip source," Nat. Commun. **11**(1), 2568 (2020).
6. G. H. Rieke, G. S. Wright, T. Böker, J. Bouwman, L. Colina, A. Glasse, K. D. Gordon, T. P. Greene, M. Güdel, Th. Henning, K. Justtanont, P.-O. Lagage, M. E. Meixner, H.-U. Nørgaard-Nielsen, T. P. Ray, M. E. Ressler, E. F. van Dishoeck, and C. Waelkens, "The Mid-Infrared Instrument for the *James Webb Space Telescope*, I: Introduction," Publ. Astron. Soc. Pac. **127**(953), 584–594 (2015).
7. C. M. Natarajan, M. G. Tanner, and R. H. Hadfield, "Superconducting nanowire single-photon detectors: physics and applications," Supercond. Sci. Technol. **25**(6), 063001 (2012).
8. I. Esmaeil Zadeh, J. Chang, J. W. N. Los, S. Gyger, A. W. Elshaari, S. Steinhauer, S. N. Dorenbos, and V. Zwiller, "Superconducting nanowire single-photon detectors: A perspective on evolution, state-of-the-art, future developments, and applications," Appl Phys Lett **118**(19), 190502 (2021).
9. L. Hao, J. C. Gallop, C. Gardiner, P. Josephs-Franks, J. C. Macfarlane, S. K. H. Lam, and C. Foley, "Inductive superconducting transition-edge detector for single-photon and macro-molecule detection," Supercond. Sci. Technol. **16**(12), 1479–1482 (2003).
10. S. Steinhauer, L. Yang, S. Gyger, T. Lettner, C. Errando-Herranz, K. D. Jöns, M. A. Baghban, K. Gallo, J. Zichi, and V. Zwiller, "NbTiN thin films for superconducting photon detectors on photonic and two-dimensional materials," Appl Phys Lett **116**(17), 171101 (2020).
11. I. Esmaeil Zadeh, J. W. N. Los, R. B. M. Gourgues, V. Steinmetz, G. Bulgarini, S. M. Dobrovolskiy, V. Zwiller, and S. N. Dorenbos, "Single-photon detectors combining high efficiency, high detection rates, and ultra-high timing resolution," APL Photonics **2**(11), 111301 (2017).
12. R. Flaschmann, L. Zugliani, C. Schmid, S. Spedicato, S. Strohauer, F. Wietschorke, F. Flassig, J. J. Finley, and K. Müller, "The dependence of timing jitter of superconducting nanowire single-photon detectors on the multi-layer sample design and slew rate," Nanoscale **15**(3), 1086–1091 (2023).
13. F. Marsili, V. B. Verma, J. A. Stern, S. Harrington, A. E. Lita, T. Gerrits, I. Vayshenker, B. Baek, M. D. Shaw, R. P. Mirin, and S. W. Nam, "Detecting single infrared photons with 93% system efficiency," Nat. Photonics **7**(3), 210–214 (2013).
14. D. Rosenberg, A. J. Kerman, R. J. Molnar, and E. A. Dauler, "High-speed and high-efficiency superconducting nanowire single photon detector array," Opt. Express **21**(2), 1440 (2013).
15. W. Zhang, L. You, H. Li, J. Huang, C. Lv, L. Zhang, X. Liu, J. Wu, Z. Wang, and X. Xie, "NbN superconducting nanowire single photon detector with efficiency over 90% at 1550 nm wavelength operational at compact cryocooler temperature," Sci. China Phys. Mech. Astron. **60**(12), 120314 (2017).
16. J. P. Sprengers, A. Gaggero, D. Sahin, S. Jahanmirinejad, G. Frucci, F. Mattioli, R. Leoni, J. Beetz, M. Lermer, M. Kamp, S. Höfling, R. Sanjines, and A. Fiore, "Waveguide superconducting single-photon detectors for integrated quantum photonic circuits," Appl. Phys. Lett. **99**(18), 181110 (2011).
17. K. M. Rosfjord, J. K. W. Yang, E. A. Dauler, A. J. Kerman, V. Anant, B. M. Voronov, G. N. Gol'tsman, and K. K. Berggren, "Nanowire single-photon detector with an integrated optical cavity and anti-reflection coating," Opt. Express **14**(2), 527 (2006).
18. F. Sterl, N. Strohfeldt, S. Both, E. Herkert, T. Weiss, and H. Giessen, "Design Principles for Sensitivity Optimization in Plasmonic Hydrogen Sensors," ACS Sens. **5**(4), 917–927 (2020).
19. M. Rigon, V. Paolucci, M. Sturaro, S. M. Emamjomeh, C. Cantalini, and A. Martucci, "Effect of Pt Nanoparticles on the Plasmonic and Chemoresistive Gas Sensing Properties of ZnO:Ga Film," in *EUROSENSORS 2018* (MDPI, 2018), p. 997.
20. X. Yin, T. Steinle, L. Huang, T. Taubner, M. Wuttig, T. Zentgraf, and H. Giessen, "Beam switching and bifocal zoom lensing using active plasmonic metasurfaces," Light: Sci. Appl. **6**(7), e17016 (2017).
21. N. Liu, M. Mesch, T. Weiss, M. Hentschel, and H. Giessen, "Infrared Perfect Absorber and Its Application As Plasmonic Sensor," Nano Lett. **10**(7), 2342–2348 (2010).
22. R. Walter, A. Tittl, A. Berrier, F. Sterl, T. Weiss, and H. Giessen, "Large-Area Low-Cost Tunable Plasmonic Perfect Absorber in the Near Infrared by Colloidal Etching Lithography," Adv Opt Mater **3**(3), 398–403 (2015).
23. N. I. Landy, S. Sajuyigbe, J. J. Mock, D. R. Smith, and W. J. Padilla, "Perfect Metamaterial Absorber," Phys. Rev. Lett. **100**(20), 207402 (2008).
24. F. Monticone and A. Alù, "Metamaterials and plasmonics: From nanoparticles to nanoantenna arrays, metasurfaces, and metamaterials," Chin. Phys. B **23**(4), 047809 (2014).
25. A. Tittl, A.-K. U. Michel, M. Schäferling, X. Yin, B. Gholipour, L. Cui, M. Wuttig, T. Taubner, F. Neubrech, and H. Giessen, "A Switchable Mid-Infrared Plasmonic Perfect Absorber with Multispectral Thermal Imaging Capability," Adv. Mater. **27**(31), 4597–4603 (2015).
26. A. Farag, M. Ubl, A. Konzelmann, M. Hentschel, and H. Giessen, "Utilizing niobium plasmonic perfect absorbers for tunable near- and mid-IR photodetection," Opt. Express **27**(18), 25012 (2019).
27. P. Karl, S. Mennle, M. Ubl, M. Hentschel, P. Flad, J.-W. Yang, T.-Y. Peng, Y.-J. Lu, and H. Giessen, "Tunable infrared high absorbing polarization independent niobium nitride plasmonic perfect absorber nanowire photodetectors," Opt. Mater. Express **12**(7), 2453 (2022).

OPTICS CONTINUUM

28. A. Tittl, P. Mai, R. Taubert, D. Dregely, N. Liu, and H. Giessen, "Palladium-Based Plasmonic Perfect Absorber in the Visible Wavelength Range and Its Application to Hydrogen Sensing," Nano Lett. **11**(10), 4366–4369 (2011).
29. T. Weiss, N. A. Gippius, S. G. Tikhodeev, G. Granet, and H. Giessen, "Efficient calculation of the optical properties of stacked metamaterials with a Fourier modal method," J. Opt. A: Pure Appl. Opt. **11**(11), 114019 (2009).
30. T. Weiss, G. Granet, N. A. Gippius, S. G. Tikhodeev, and H. Giessen, "Matched coordinates and adaptive spatial resolution in the Fourier modal method," Opt. Express **17**(10), 8051 (2009).
31. P. Ruchka, S. Hammer, M. Rockenhäuser, R. Albrecht, J. Drozella, S. Thiele, H. Giessen, and T. Langen, "Microscopic 3D printed optical tweezers for atomic quantum technology," Quantum Sci. Technol. **7**(4), 045011 (2022).
32. M. Sartison, K. Weber, S. Thiele, L. Bremer, S. Fischbach, T. Herzog, S. Kolatschek, M. Jetter, S. Reitzenstein, A. Herkommer, P. Michler, S. L. Portalupi, and H. Giessen, "3D printed micro-optics for quantum technology: Optimised coupling of single quantum dot emission into a single-mode fibre," Light: Advanced Manufacturing **2**(2), 103 (2021).